

## Article

# New Bioprecursor Prodrugs of Sulfadiazine: Synthesis, X-ray Structure and Hirshfeld Analysis

Mezna Saleh Altowyan <sup>1</sup>, Saied M. Soliman <sup>2</sup>, Magda M. F. Ismail <sup>3</sup>, Matti Haukka <sup>4</sup>, Assem Barakat <sup>5,\*</sup>  
and Mohammed Salah Ayoup <sup>2,\*</sup>

<sup>1</sup> Department of Chemistry, College of Science, Princess Nourah bint Abdulrahman University, P.O. Box 84428, Riyadh 11671, Saudi Arabia; msaltowyan@pnu.edu.sa

<sup>2</sup> Department of Chemistry, Faculty of Science, Alexandria University, P.O. Box 426, Alexandria 21321, Egypt; saeed.soliman@alexu.edu.eg

<sup>3</sup> Department of Pharmaceutical Medicinal Chemistry, Faculty of Pharmacy (Girls), Al-Azhar University, Cairo 11651, Egypt; magdaismail@azhar.edu.eg

<sup>4</sup> Department of Chemistry, University of Jyväskylä, P.O. Box 35, FI-40014 Jyväskylä, Finland; matti.o.haukka@jyu.fi

<sup>5</sup> Department of Chemistry, College of Science, King Saud University, P.O. Box 2455, Riyadh 11451, Saudi Arabia

\* Correspondence: ambarakat@ksu.edu.sa (A.B.); mohamed.salah@alexu.edu.eg (M.S.A.); Tel.: +966-11467-5901 (A.B.); Fax: +966-11467-5992 (A.B.)

**Abstract:** Sulphonamide motif is found extensively in numerous chemotherapeutic drug candidates, it acts by stopping the production of folate inside the bacterial cell. Current research has established the synthesis and characterization of new bioprecursor prodrugs of sulfadiazine. The first prodrug, **3**, was synthesized via the coupling of diazonium salt of sulfadiazine with ethyl acetoacetate in AcONa at 0 °C. The second prodrug, sulfadiazine-pyrazole, **5**, was furnished via cyclocondensation of the hydrazono derivative, **3**, and 2-pyridyl hydrazine, **4**. The generated data from the X-ray analysis is interpreted and refined to obtain the crystal structure of the target compound, **5**. Density functional theory (DFT) method was used to calculate the optimized geometrical parameters, electronic state (HOMO–LUMO), and the electronic properties. Moreover, Hirshfeld analysis revealed that the most important contributions to the crystal packing of the prodrug **5** are H···H, O···H and H···C contacts.

**Keywords:** bioprecursor prodrug; sulfadiazine; computational studies; Hirshfeld



**Citation:** Altowyan, M.S.; Soliman, S.M.; Ismail, M.M.F.; Haukka, M.; Barakat, A.; Ayoup, M.S. New Bioprecursor Prodrugs of Sulfadiazine: Synthesis, X-ray Structure and Hirshfeld Analysis. *Crystals* **2022**, *12*, 1016. <https://doi.org/10.3390/cryst12081016>

Academic Editor: Changquan Calvin Sun

Received: 15 June 2022

Accepted: 19 July 2022

Published: 22 July 2022

**Publisher's Note:** MDPI stays neutral with regard to jurisdictional claims in published maps and institutional affiliations.



**Copyright:** © 2022 by the authors. Licensee MDPI, Basel, Switzerland. This article is an open access article distributed under the terms and conditions of the Creative Commons Attribution (CC BY) license (<https://creativecommons.org/licenses/by/4.0/>).

## 1. Introduction

Sulfonamides inhibit bacterial folate biosynthesis and have been extensively used as broad-spectrum antimicrobials for decades, making use of the different metabolic pathways of microbial and human cells. Nonetheless, bacteria invariably develop resistance to any introduced therapy and only drug combinations, currently used in clinic, can effectively combat the multidrug-resistant (MDR) [1]. Inherent and developed resistance modes of bacteria to antibiotics are problems in the design of new drugs. In the era of bacterial resistance, a prodrug strategy can be employed that requires bacterium-specific enzymes to release the active drug at the infection site. Therefore, targeting the prodrugs to a specific enzyme has potential as a selective drug delivery system in microbial chemotherapy [2,3]. Additionally, prodrugs may enhance the pharmacological activity or pharmacokinetic properties of a parent drug molecule.

The azo group/sulphonamide hybrid structure was the first well-organized chemotherapeutic agent that could be applied efficiently for the treatment of infections caused by bacteria in humans. Prontosil (**I**, Figure 1) was recognized as a bioprecursor to the active compound, sulfanilamide, possibly metabolized by azoreductases released either in the liver or by gut microbiota [4,5]. Azoreductases are flavoenzymes that have been distinguished in a range of prokaryotes and eukaryotes [6]. Gaffer et al. [7] explored the synthetic

methodology of new amino-thiazolylazo-sulphonamide (**II**). The synthesized dyes were investigated for their anti-bacterial and anti-fungal activities against Gram-positive and Gram-negative bacteria, as well as a fungi (*C. albicans*).

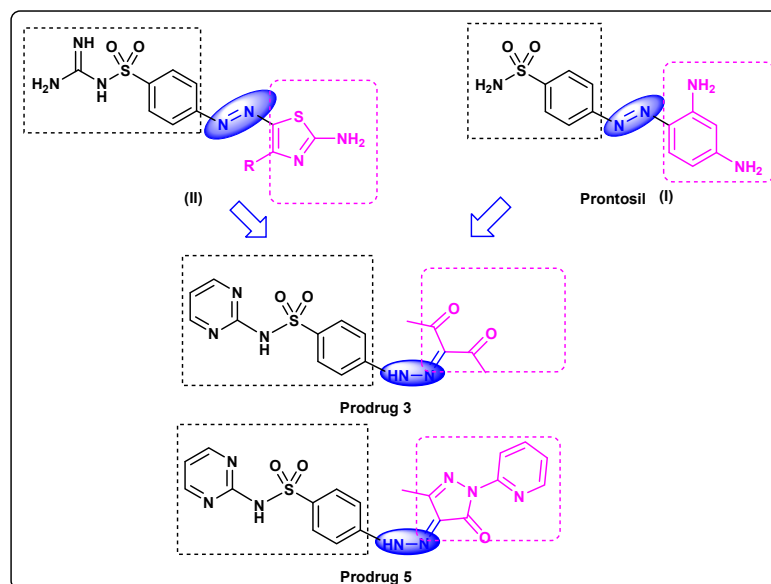


**Figure 1.** Feature similarities between leads **I**, **II** and target compound.

Sulfadiazine (2-sulfanilamidopyrimidine) is used to a large extent for the elimination of bacteria that cause urinary tract infections. It is also used in combined therapy with pyrimethamine and folinic acid for the treatment of some parasitic diseases such as malaria and toxoplasmosis. Silver sulfadiazine is an efficient prescription for burn and wounds treatment [1]; in addition, it has been prescribed for treating bacterial infections, e.g., otitis media, encephalitis, and severe meningococcal meningitis, besides its role as a prophylactic treatment for rheumatic fever. Sulfadiazine targets the dihydropyruvate synthase (DHPS), producing a bacteriostatic effect, with a wide spectrum against most Gram-positive and many Gram-negative organisms [1,8].

As a continuation to our research on sulfa drugs [9–11], our current research focus is on sulfadiazine [12], a model scaffold to discover new sulfadiazine bioprecursors. Herein, novel models have been designed which feature similarities between our target compounds and lead compounds, as clarified in Figure 1. They are synthesized and characterized by microanalytical analyses,  $^1\text{H}$ NMR and  $^{13}\text{C}$ NMR. Particularly, sulfadiazine-pyrazole prodrug **5** is further investigated via X-ray single crystal diffraction which provides the screening, testing, and complete data collection. Furthermore, density functional methods (DFT) will be applied to achieve a valuable understanding of the electronic and molecular properties of the target **5**.

## 2. Materials and Instrumentations

### 2.1. Materials and Equipments

All materials and instruments are given in Supplementary materials.

### 2.2. Synthesis of (E)-4-(2-(3-Methyl-5-oxo-1-(pyridin-2-yl)-1H-pyrazol-4(5H)-ylidene)hydrazinyl)-N-(pyrimidin-2-yl)benzenesulfonamide (**5**)

Synthesis of compound **3** was performed according to the method reported in the literature as described in Supplementary materials [12]. Then, a solution of the hydrazino **3** (1.0 mmol) in absolute EtOH (10 mL), 2-hydrazinopyridine **4** (1.2 mmol) was added, and the mixture was then allowed to reflux for 8 h, before the formed precipitate was collected by filtration, recrystallized from EtOH to create pale yellow crystals, (270 mg, 62%), m.p = 292–294 °C  $^1\text{H}$ NMR (500 MHz, DMSO- $d_6$ )  $\delta_{\text{H}}$ : 13.03 (bs, 1H, N-H), 11.81 (bs,

1H, N-H), 8.47 (d,  $J = 4.5$  Hz, 2H, Ar-H), 8.41 (d,  $J = 3.0$  Hz, 1H, Ar-H), 7.98 (d,  $J = 9.0$  Hz, 2H, Ar-H), 7.87 (t,  $J = 8.5$  Hz, 1H, Ar-H), 7.78 (d,  $J = 8.0$  Hz, 1H, Ar-H), 7.70 (d,  $J = 9.0$  Hz, 2H, Ar-H), 7.22 (t,  $J = 7.5$  Hz, 1H, Ar-H), 7.01 (t,  $J = 6.5$  Hz, 1H, Ar-H), 2.23 (s, 3H, CH<sub>3</sub>); <sup>13</sup>C NMR (125 MHz, DMSO-*d*<sub>6</sub>)  $\delta_C$ : 158.9, 157.3, 156.9, 149.8, 149.4, 148.9, 145.4, 138.9, 136.5, 129.9, 121.7, 116.3, 114.5 (Ar-C), 12.2 (CH<sub>3</sub>); Anal. Calcd. for C<sub>19</sub>H<sub>16</sub>N<sub>8</sub>O<sub>3</sub>S: C, 52.29; H, 3.70; N, 25.67; Found C, 52.47; H, 3.91; N, 25.42.

### 2.3. X-ray Structure Analyses

The accomplished utilizing of **5** was determined using the method described in Supplementary data [13–16]. The crystal data are given in Table 1. Analysis of the crystal packing was accomplished utilizing using Crystal Explorer 17.5 program [17].

**Table 1.** Data of the Crystal **5**.

5	
CCDC	2179179
empirical formula	C <sub>19</sub> H <sub>16</sub> N <sub>8</sub> O <sub>3</sub> S
fw	436.46
temp (K)	120(2) K
$\lambda$ (Å)	1.54184 Å
cryst syst	Monoclinic
space group	C2/c
$a$ (Å)	21.8909(2) Å
$b$ (Å)	11.45860(10) Å
$c$ (Å)	15.77880(10) Å
$\beta$ (deg)	99.0430(10)°
$V$ (Å <sup>3</sup> )	3908.74(6) Å <sup>3</sup>
$Z$	8
$\rho_{\text{calc}}$ (Mg/m <sup>3</sup> )	1.483 Mg/m <sup>3</sup>
$\mu$ (Mo K $\alpha$ ) (mm <sup>-1</sup> )	1.839 mm <sup>-1</sup>
No. reflections.	33705
Unique reflns.	4133
Completeness to $\theta = 67.684^\circ$	99.9%
GOOF ( $F^2$ )	1.054
$R_{\text{int}}$	0.0241
$R_1^a$ ( $I \geq 2\sigma$ )	0.0368
$wR_2^b$ ( $I \geq 2\sigma$ )	0.1045

$$^a R_1 = \sum ||F_o| - |F_c|| / \sum |F_o|. \quad ^b wR_2 = \{\sum [w(F_o^2 - F_c^2)^2] / \sum [w(F_o^2)]\}^{1/2}.$$

### 2.4. Computational Methods

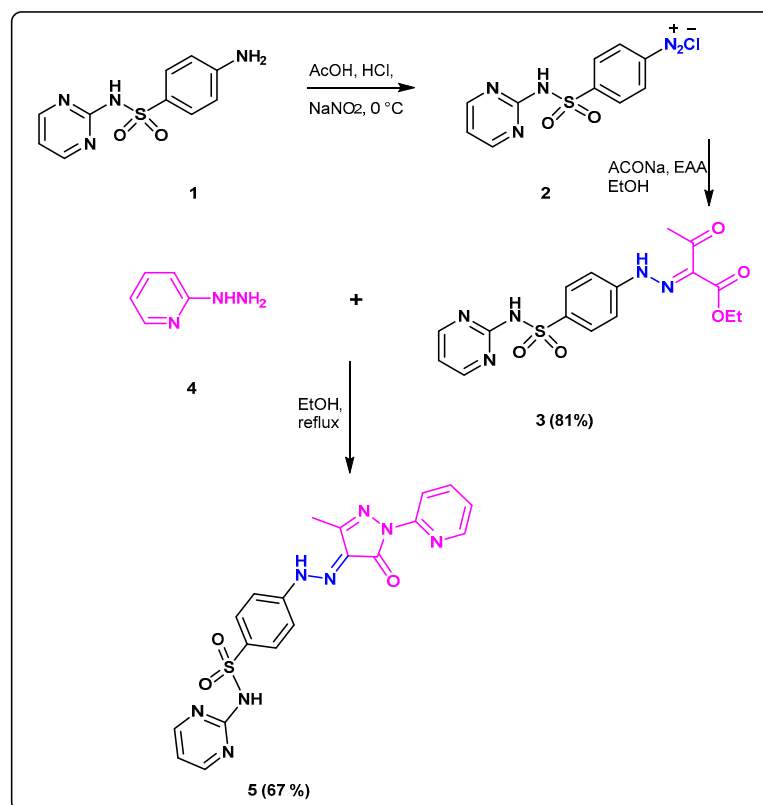
All theoretical details are described in Supplementary materials [18–20].

## 3. Results and Discussion

### 3.1. Chemistry

The facile synthetic protocol was performed for preparation of new sulfadiazine pro-drug **5** (Scheme 1). Reaction of the sulfadiazine **1** with the solution of NaNO<sub>2</sub> to accomplish the diazotization step at 0 °C at pH = 2–3 afforded the corresponding diazonium salt **2** as a clear solution. The coupling of **2** with the previously prepared carbanion salt of ethylacetoacetate at 0 °C gave the desired hydrazono-ethylacetoacetate **3**. Confirmation of the correct structure **3** was accomplished by the spectroscopic analysis where <sup>1</sup>H NMR provided two separate peaks at  $\delta_H$ : 11.72 and 11.53 ppm correspond to two N-H protons, as well as two non-homotopic protons signals at 4.26 and 1.22 ppm representing two types of ethyl protons. Furthermore, the singlet signal at  $\delta_H$ : 2.38 revealed to CH<sub>3</sub>CO; <sup>13</sup>C NMR spectra of **3** showed two different types of C=O at  $\delta_C$ : 194.5 and 162.7 beside two different signals at  $\delta_C$  25.7, 14.1 ppm revealed to carbons of two non-homotopic CH<sub>3</sub>. Cyclocondensation of the prodrug **3** with 2-hydrazinopyridine **4** was accomplished by heating in absolute EtOH affording the desired sulfadiazinepyrazolo prodrugs derivative **5**. Confirmation of

the correct structure of the sulfonamide **5** was accomplished by the spectroscopic analysis where  $^1\text{H}$ NMR gave characteristic signals at  $\delta_{\text{H}}$ : 13.03 and 11.81 ppm revealed to two different sets of NH protons beside one signals in the aliphatic region at  $\delta_{\text{H}}$ : 2.23 ppm representing to  $\text{CH}_3$  also  $^{13}\text{C}$  NMR of **5** showed 3 types of carbonyl carbons at  $\delta_{\text{C}}$ : 158.9, as well one signal in aliphatic region at  $\delta_{\text{C}}$  12.2 ppm corresponded to  $\text{CH}_3$  carbons.



**Scheme 1.** Synthesis of the target prodrugs **3** and **5**.

### 3.2. The Description of X-ray Structure of **5**

The X-ray structure of **5** shown in Figure 2A agreed very well with its spectral data. It crystallized in the monoclinic  $C2/c$  space group. There are eight molecules per unit cell and one molecular unit as an asymmetric formula. The unit cell parameters are  $a = 21.8909(2)$  Å,  $b = 11.45860(10)$  Å,  $c = 15.77880(10)$  Å,  $\beta = 99.0430(10)^\circ$  and  $V = 3908.74(6)$  Å<sup>3</sup>. Selected geometric parameters are depicted in Table 2. The pyridyl and the five membered rings are connected to one another by C(5)-N(2) bond where both rings are twisted from one another by only  $6.45^\circ$ . On the other hand, the phenyl moiety is found twisted further from the five membered ring mean plane. The twist angle in this case is  $23.30^\circ$ .

The molecular structure of **5** is stabilized by the N(5)-H(5)⋯O(1) intramolecular H-bond while the crystal is packed in by the N(6)-H(6)⋯N(3) intermolecular H-bond (Figure 2B). The donor-acceptor distance is 2.793(2) and 2.932(2) Å, respectively (Table 3). The packing of these molecular units showed a 1D hydrogen bonding polymer extended along the  $a$ -direction (Figure 2C).

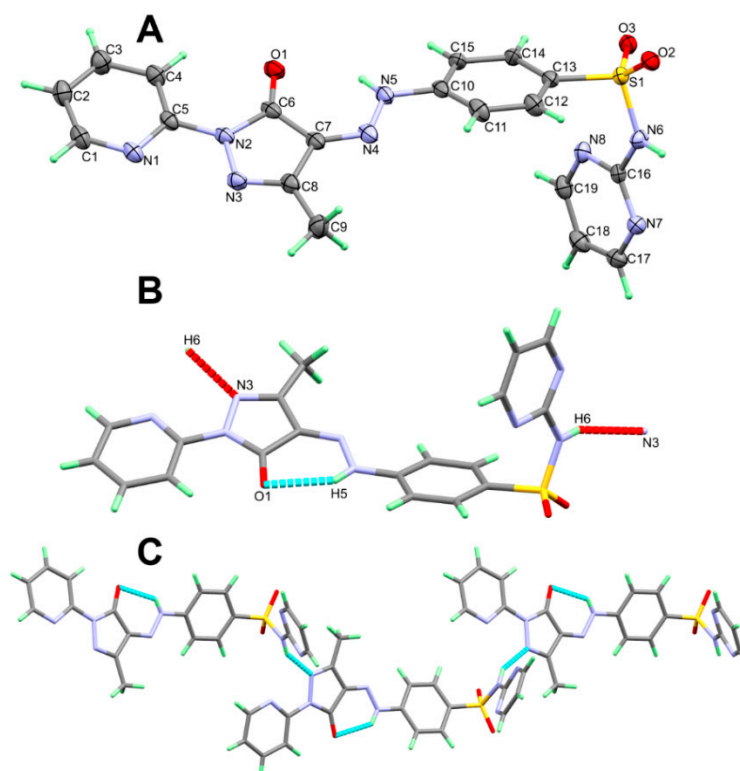


**Figure 2.** The asymmetric formula (A), H-bond contacts (B) and packing (C) of 5.

**Table 2.** Selected geometric parameters [Å and °] for 5.

Atoms	Distance	Atoms	Distance
S(1)-O(3)	1.4264(11)	N(1)-C(1)	1.341(2)
S(1)-O(2)	1.4330(11)	N(2)-C(6)	1.3857(18)
S(1)-N(6)	1.6338(13)	N(2)-C(5)	1.407(2)
S(1)-C(13)	1.7600(15)	N(2)-N(3)	1.4113(18)
O(1)-C(6)	1.232(2)	N(3)-C(8)	1.302(2)
N(1)-C(5)	1.3377(19)	N(4)-C(7)	1.309(2)
Atoms	Angle	Atoms	Angle
O(3)-S(1)-O(2)	118.70(7)	C(5)-N(1)-C(1)	116.22(15)
O(3)-S(1)-N(6)	110.78(7)	C(6)-N(2)-C(5)	128.94(14)
O(2)-S(1)-N(6)	103.46(7)	C(6)-N(2)-N(3)	111.73(13)
O(3)-S(1)-C(13)	108.38(7)	C(5)-N(2)-N(3)	119.17(12)
O(2)-S(1)-C(13)	109.69(7)	C(8)-N(3)-N(2)	107.33(12)
N(6)-S(1)-C(13)	104.95(7)	C(7)-N(4)-N(5)	118.00(16)

**Table 3.** Hydrogen bonds for prodrug 5 [Å and °].

D-H...A	d(D-H)	d(H...A)	d(D...A)	<(DHA)
N(5)-H(5)...O(1)	0.816(17)	2.162(17)	2.793(2)	134.3(15)
N(6)-H(6)...N(3)#1	0.89(2)	2.15(2)	2.932(2)	146.6(19)

Symm. Code: #1  $x + 1/2, -y + 1/2, z + 1/2$ .

### 3.3. Hirshfeld Surface Analysis

The Hirshfeld calculation is a simple and accurate tool for the finding the different atom–atom contacts in the crystal structure. Hence, decomposition of the different intermolecular contacts in the crystal structure of 5 was performed using Hirshfeld calculations. The resulting Hirshfeld maps are presented in Figure 3. There are different levels of inter-

molecular contacts as indicated from the presence of red, white, and blue regions in the  $d_{\text{norm}}$  map.

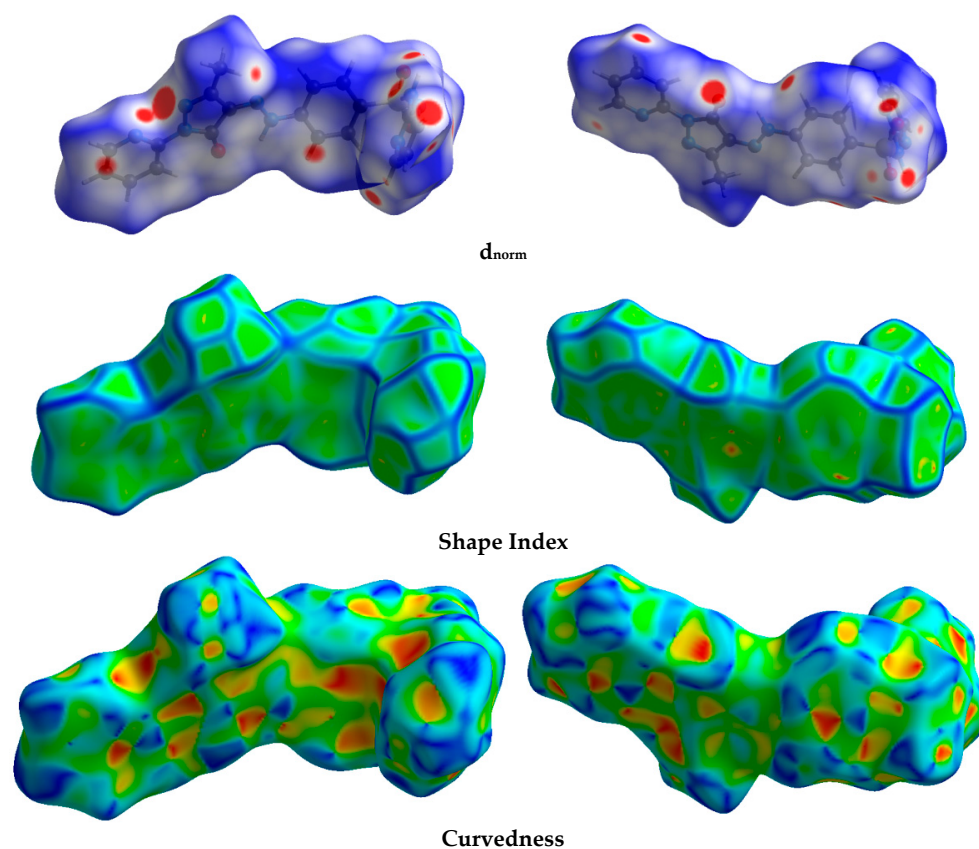


**Figure 3.** Hirshfeld surfaces of prodrug 5.

Analysis of these interactions using fingerprint plot is given in Figure 4. The fingerprint area gave the percentages of all intermolecular interactions in the crystal structure of 5. Presentation for these interactions and the percentages for all contacts in 5 is shown in Figure 5. The percentages of the H...H, H...C, N...H, and O...H interactions are 36.4, 12.2, 17.3, and 16.9%, respectively. It is worth noting that the N...H and O...H contacts have small interaction distances (Table 4). In addition, the presence of  $\pi$ - $\pi$  stacking interactions is revealed by the presence of short C1...C15 contact (3.211 Å) and the presence of red/blue triangles in the shape index map and flat green area in curvedness (Figure 3).

**Table 4.** Short contacts in 5.

Contact	Distance	Contact	Distance
O(3) ... H3A	2.354	O(2) ... H(12)	2.396
O(3) ... H18	2.530	N(7) ... H(15)	2.397
O(2) ... H19	2.360	N(1) ... H(6)	2.430
O(1) ... H17	2.218	N(3) ... H(6)	2.048
O(3) ... H9B	2.473	C(1) ... C(15)	3.211
O(2) ... H19	2.360		

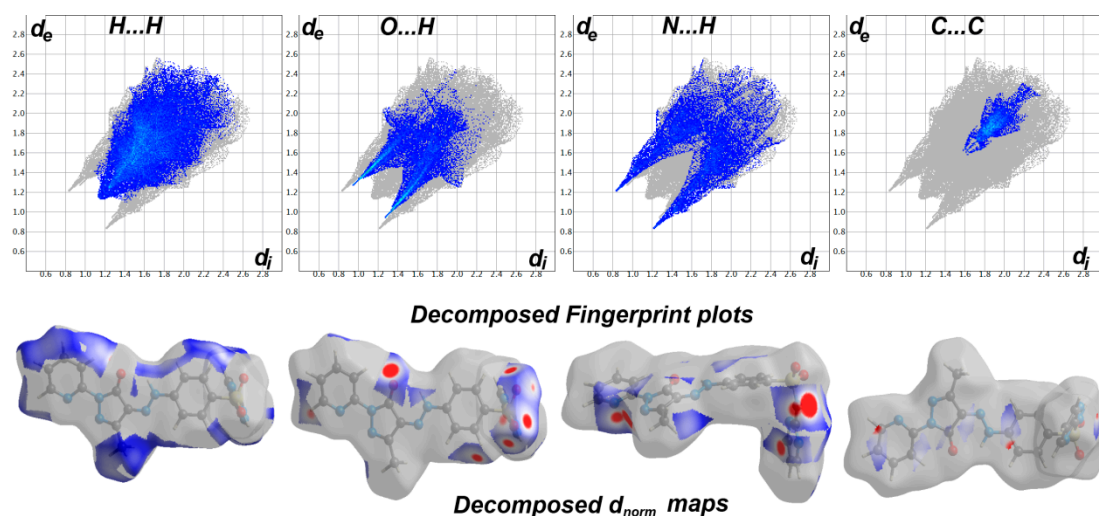


Figure 4. Fingerprint plots and decomposed  $d_{norm}$  maps in 5.

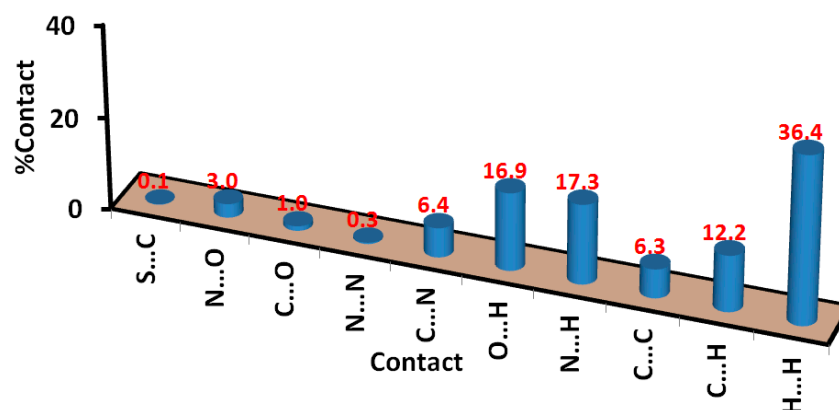


Figure 5. Intermolecular contacts and their percentages in prodrug 5.

### 3.4. DFT Studies

The minimum energy structure of 5 is shown in Figure 6. Its overlay with the X-ray geometry is shown in the same figure. Generally, there is structural matching between both structures and also good correlations between the optimized and X-ray geometric parameters (Figure 7) which reveal these observations very well (Table S1, Supporting information).

Natural charges of 5 shown in Figure 8 indicate that the O, N, and most of C-atoms are electronegative. The O-sites have charges ranging from  $-0.6363$  to  $-0.9475$  e where the most negative oxygen sites are those for the sulphonyl group. The corresponding S-atom is the most electropositive ( $2.3582$  e). Regarding carbon atoms, C39 ( $0.5956$  e) which is bonded to three nitrogen atoms and the carbonyl carbon ( $0.6173$  e) is the most electropositive carbon site. In contrast, all the H-atoms are charged positively where the H46 ( $0.4409$  e) and H47 ( $0.4617$  e) are the most positive hydrogen sites. Presentation of electrostatic potential (MEP) is shown in Figure 9. The molecule has a net dipole moment of  $4.9143$  D.

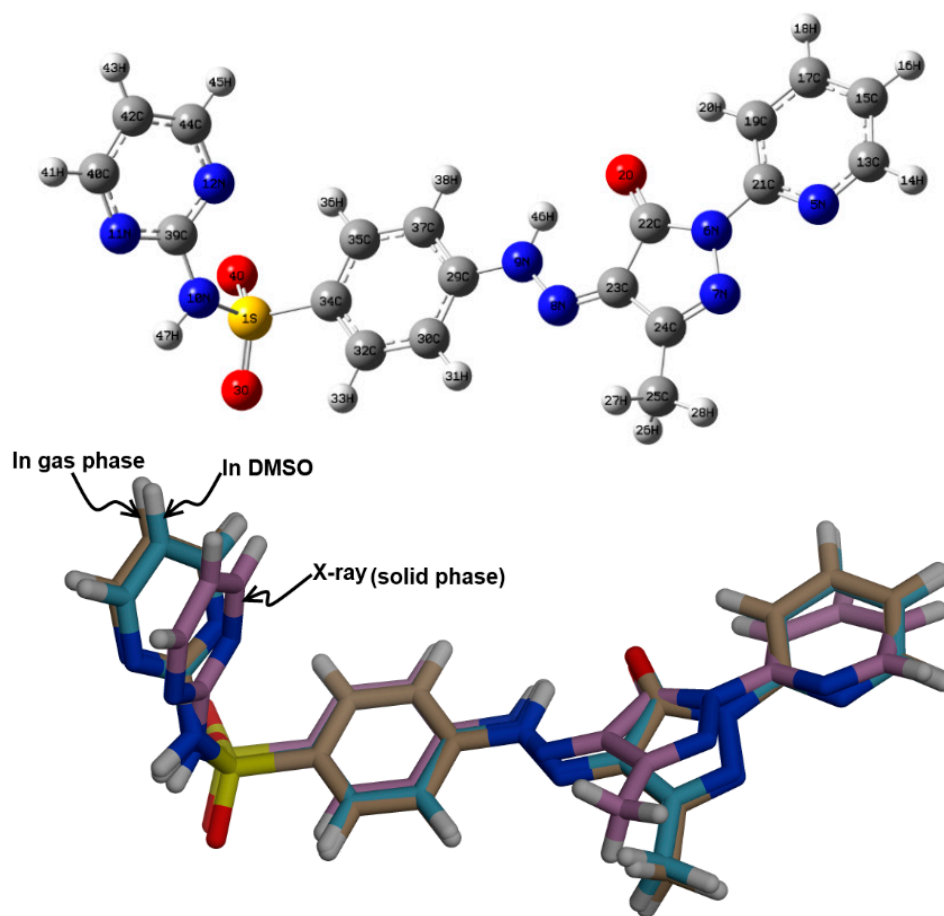


Figure 6. The minimum energy structure (**upper**) compared with the X-ray structure (**lower**) of 5.

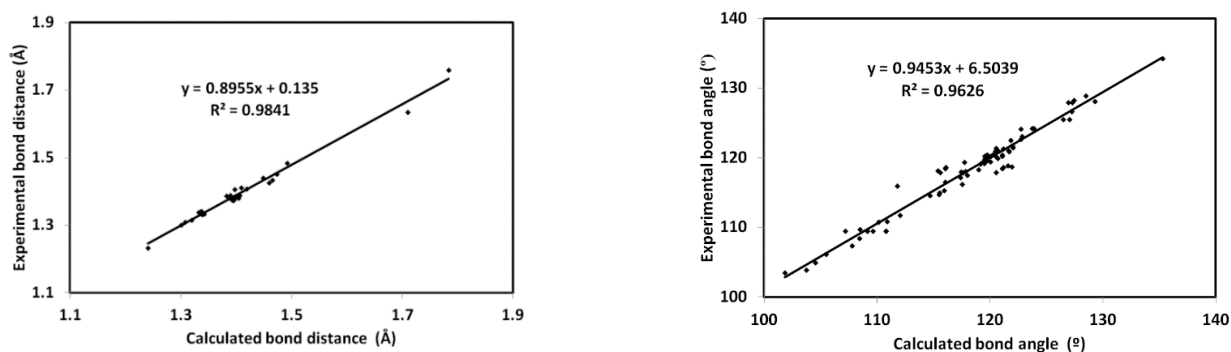


Figure 7. Correlations between the optimized and X-ray geometric parameters.

Among electronic parameters which play an important role are the HOMO and LUMO levels. These molecular orbitals are shown in Figure 9. It is clear that both are distributed over the  $\pi$ -system of the molecule. Hence, the HOMO $\rightarrow$ LUMO excitation is mainly a  $\pi\text{-}\pi^*$  transition. Their energies are calculated to be  $-6.1158$  and  $-2.7671$  eV, respectively, and the HOMO–LUMO gap is 3.3487 eV. As a result, the reactivity indices [21–27] such as ionization potential (I), electron affinity (A), hardness ( $\eta$ ), electrophilicity index ( $\omega$ ) and chemical potential ( $\mu$ ) are calculated to be 6.1158, 2.7671, 3.3487, 2.9455 and  $-4.4415$  eV, respectively.

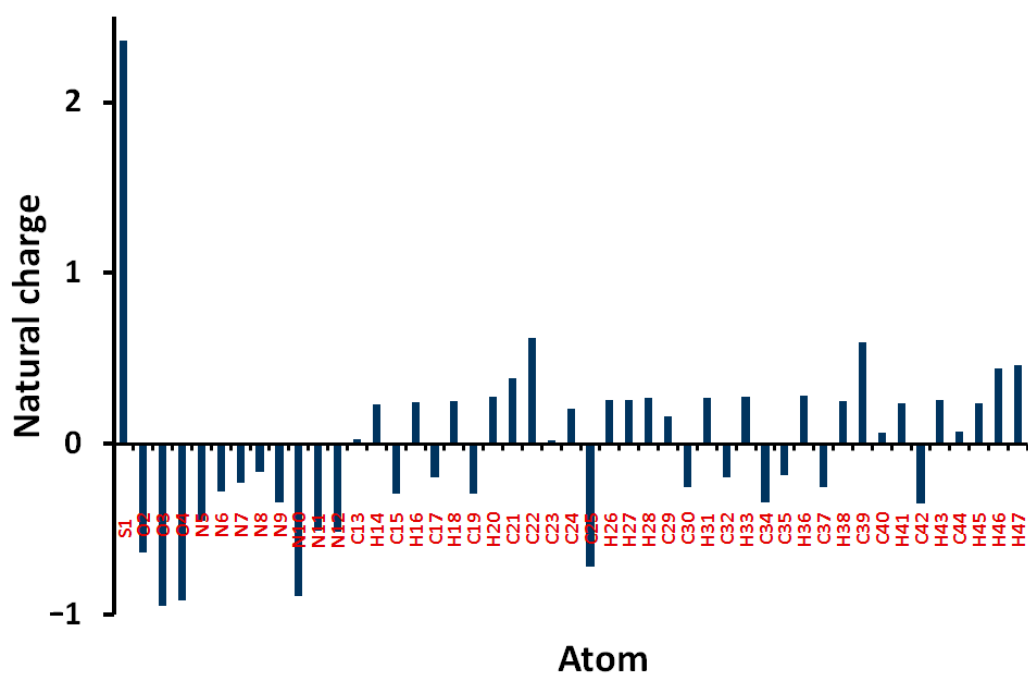


Figure 8. Atomic charges in 5.

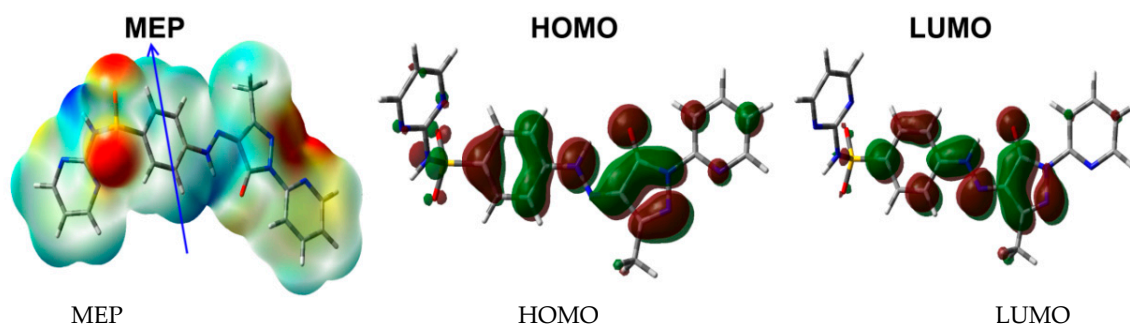


Figure 9. The MEP, HOMO, and LUMO of 5.

### 3.5. NBO Analysis

The delocalization of the electron processes has a greatly effective role in the molecule stability [28–30]. There are many  $\pi \rightarrow \pi^*$ ,  $n \rightarrow \sigma^*$ ,  $\sigma \rightarrow \sigma^*$  and  $n \rightarrow \pi^*$  electron delocalization processes which stabilize the structure (Table 5). The stabilization energies ( $E^{(2)}$ ) of the  $\sigma \rightarrow \sigma^*$  and  $\pi \rightarrow \pi^*$  processes are in the range of 4.25–4.69 and 6.18–35.16 kcal/mol. The  $\text{BD}(2)\text{N11}-\text{C40} \rightarrow \text{BD}^*(2)\text{N12}-\text{C39}$  (35.16 kcal/mol) and  $\text{BD}(2)\text{C42}-\text{C44} \rightarrow \text{BD}^*(2)\text{N11}-\text{C40}$  (34.43 kcal/mol) are the strongest electron delocalization processes. In addition, the  $\text{LP}(2)\text{O2} \rightarrow \text{BD}^*(1)\text{N6}-\text{C22}$  (26.42 kcal/mol) and  $\text{LP}(1)\text{N6} \rightarrow \text{BD}^*(2)\text{N5}-\text{C21}$  (38.97 kcal/mol) are the strongest  $n \rightarrow \sigma^*$  and  $n \rightarrow \pi^*$  electron delocalization processes, respectively.

**Table 5.** Electron delocalization processes in **5**<sup>a</sup>.

(NBO) <sub>i</sub> <sup>b</sup>	(NBO) <sub>j</sub> <sup>c</sup>	E <sup>(2)</sup>	(NBO) <sub>i</sub> <sup>b</sup>	(NBO) <sub>j</sub> <sup>c</sup>	E <sup>(2)</sup>
BD(1) N 5-C13	BD*(1) N 6-C21	4.69	LP(2) O 2	BD*(1) N 6-C22	26.42
BD(1) N11-C40	BD*(1) N10-C39	4.54	LP(2) O 2	BD*(1) C22-C23	15.47
BD(1) N12-C44	BD*(1) N10-C39	4.65	LP(2) O 3	BD*(1) S 1-N10	11.45
BD(1) C23-C24	BD*(1) O 2-C22	4.25	LP(2) O 3	BD*(1) S 1-C34	16.98
BD(2) N 5-C21	BD*(2) C13-C15	26.23	LP(3) O 3	BD*(1) S 1-O 4	19.91
BD(2) N 5-C21	BD*(2) C17-C19	12.15	LP(3) O 3	BD*(1) S 1-N10	13.36
BD(2) N 7-C24	BD*(2) N 8-C23	13.42	LP(2) O 4	BD*(1) S 1-O 3	5.62
BD(2) N 8-C23	BD*(2) N 7-C24	14.46	LP(2) O 4	BD*(1) S 1-N10	8.73
BD(2) N 8-C23	BD*(2) N 8-C23	6.18	LP(2) O 4	BD*(1) S 1-C34	18.62
BD(2) N11-C40	BD*(2) N12-C39	35.16	LP(3) O 4	BD*(1) S 1-O 3	16.79
BD(2) N11-C40	BD*(2) C42-C44	10.11	LP(3) O 4	BD*(1) S 1-N10	22.05
BD(2) N12-C39	BD*(2) N11-C40	9.19	LP(1) N 5	BD*(1) C13-C15	9.60
BD(2) N12-C39	BD*(2) C42-C44	30.90	LP(1) N 5	BD*(1) C19-C21	10.67
BD(2) C13-C15	BD*(2) N 5-C21	16.36	LP(1) N 7	BD*(1) N 6-C22	6.08
BD(2) C13-C15	BD*(2) C17-C19	23.01	LP(1) N 7	BD*(1) C23-C24	7.07
BD(2) C17-C19	BD*(2) N 5-C21	28.00	LP(1) N 8	BD*(1) C22-C23	12.04
BD(2) C17-C19	BD*(2) C13-C15	16.62	LP(1) N10	BD*(1) S 1-O 4	6.66
BD(2) C29-C37	BD*(2) C30-C32	15.87	LP(1) N10	BD*(1) S 1-C34	4.66
BD(2) C29-C37	BD*(2) C34-C35	25.53	LP(1) N11	BD*(1) N12-C39	13.62
BD(2) C30-C32	BD*(2) C29-C37	23.08	LP(1) N11	BD*(1) C40-C42	9.04
BD(2) C30-C32	BD*(2) C34-C35	16.50	LP(1) N12	BD*(1) N11-C39	13.60
BD(2) C34-C35	BD*(2) C29-C37	15.90	LP(1) N12	BD*(1) C42-C44	8.91
BD(2) C34-C35	BD*(2) C30-C32	22.37	LP(1) N 6	BD*(2) N 5-C21	38.97
BD(2) C42-C44	BD*(2) N11-C40	34.43	LP(1) N 6	BD*(2) N 7-C24	19.69
BD(2) C42-C44	BD*(2) N12-C39	12.76	LP(1) N 9	BD*(2) N 8-C23	46.68
			LP(1) N 9	BD*(2) C29-C37	35.67
			LP(1) N10	BD*(2) N12-C39	37.38

<sup>a</sup> Atom numbering refer to Figure 5; <sup>b</sup> Donor NBO and <sup>c</sup> Acceptor NBO.

#### 4. Conclusions

The novel bioprecursor prodrugs of sulfadiazine have been synthesized and evidenced through the elemental and spectral analyses “FT-IR, <sup>1</sup>HNMR, <sup>13</sup>CNMR, and MS”. More structural elucidations of the prodrug **5** were determined via X-ray and its supramolecular structure aspects were analyzed using Hirshfeld calculations. Additionally, the natural charge distribution, dipole moment, HOMO, LUMO, and MEP map of **5** were analyzed based on B3LYP/6-31G (d,p) calculations. Its structural aspects were investigated using DFT and NBO calculations.

**Supplementary Materials:** The following are available online at <https://www.mdpi.com/article/10.3390/cryst12081016/s1>, NMR spectrum; Table S1: The calculated geometric parameters of **5**<sup>a</sup>. Table S2: The calculated natural charges of **5**<sup>a</sup>.

**Author Contributions:** Conceptualization, M.S.A. (Mohammed Salah Ayoup), A.B. and S.M.S.; methodology, M.S.A. (Mohammed Salah Ayoup) and A.B.; software, S.M.S. and M.H.; validation, M.S.A. (Mezna Saleh Altowyan) and M.M.F.I.; formal analysis, M.S.A. (Mohammed Salah Ayoup), M.M.F.I. and M.H.; investigation, M.S.A. (Mohammed Salah Ayoup); resources, M.S.A. (Mezna Saleh Altowyan) and A.B.; data curation, A.B. and S.M.S.; writing—original draft preparation, M.S.A. (Mohammed Salah Ayoup), A.B. and S.M.S.; writing—review and editing, A.B. and S.M.S.; visualization, A.B. and M.S.A. (Mohammed Salah Ayoup); supervision, A.B. and M.S.A. (Mezna Saleh Altowyan); project administration, M.S.A. (Mezna Saleh Altowyan); funding acquisition, M.S.A. (Mezna Saleh Altowyan). All authors have read and agreed to the published version of the manuscript.

**Funding:** Princess Nourah bint Abdulrahman University Researchers Supporting Project number (PNURSP2022R86), Princess Nourah bint Abdulrahman University, Riyadh, Saudi Arabia.

**Institutional Review Board Statement:** Not applicable.

**Informed Consent Statement:** Not applicable.

**Data Availability Statement:** Not applicable.

**Acknowledgments:** Princess Nourah bint Abdulrahman University Researchers Supporting Project number (PNURSP2022R86), Princess Nourah bint Abdulrahman University, Riyadh, Saudi Arabia.

**Conflicts of Interest:** The authors declare no conflict of interest.

## References

1. Villa, D.F.; Aguilar, M.R.; Rojo, L. Folic Acid Antagonists: Antimicrobial and Immunomodulating Mechanisms and Applications. *Int. J. Mol. Sci.* **2019**, *20*, 4996. [CrossRef] [PubMed]
2. Koshti, S.; Patil, P.A.; Patil, C.B.; Patil, A.S. Synthesis and Characterization of Prodrugs of Sulfonamides as an Azo Derivatives of Carvacrol. *Der. Pharma. Chem.* **2018**, *10*, 1–15.
3. Pradere, U.; Garnier-Amblard, E.C.; Coats, S.J.; Amblard, F.; Schinazi, R.F. Synthesis of Nucleoside Phosphate and Phosphonate Prodrugs. *Chem. Rev.* **2014**, *114*, 9154–9218. [CrossRef] [PubMed]
4. Cheng, A.V.; Wuest, W.M. Signed, Sealed, Delivered: Conjugate and Prodrug Strategies as Targeted Delivery Vectors for Antibiotics. *ACS Infect Dis.* **2019**, *14*, 816–828. [CrossRef] [PubMed]
5. Gingell, R.; Bridges, J.W.; Williams, R.T. The Role of the Gut Flora in the Metabolism of Prontosil and Neoprontosil in the Rat. *Xenobiotica* **1971**, *1*, 143–156. [CrossRef]
6. Ryan, A. Azoreductases in drug metabolism. *Br. J. Pharmacol.* **2017**, *174*, 2161–2173. [CrossRef]
7. Gaffer, H.E. Antimicrobial sulphonamide azo dyes. *Coloration Technol.* **2019**, *135*, 484–500. [CrossRef]
8. Gündüz, M.G.; Tahir, M.N.; Armakovic, S.; Koçak, C.O.; Armakovic, S.J. Design, synthesis and computational analysis of novel acridine-(sulfadiazine/sulfathiazole) hybrids as antibacterial agents. *J. Mol. Struct.* **2019**, *1186*, 39–49. [CrossRef]
9. Ayoup, M.S.; Soliman, S.M.; Haukka, M.; Harras, M.F.; Menofy, N.G.E.; Ismail, M.M.F. Prodrugs of sulfacetamide: Synthesis, X-ray structure, Hirshfeld analysis, antibacterial assessment, and docking studies. *J. Mol. Struct.* **2022**, *1251*, 132017. [CrossRef]
10. Ismail, M.M.F.; Ghorab, M.M.; Noaman, E.; Ammar, Y.A.; Heiba, H.I.; Sayed, M.Y. Novel synthesis of pyrrolo[2,3-d]pyrimidines bearing sulfonamide moieties as potential antitumor and radioprotective agents. *Arzneim.-Forsch./Drug Res.* **2006**, *56*, 301–308. [CrossRef]
11. Ghorab, M.M.; Noaman, E.; Ismail, M.M.F.; Heiba, H.I.; Ammar, Y.A.; Sayed, M.Y. Novel Antitumor And Radioprotective Sulfonamides Containing Pyrrolo[2,3-D]Pyrimidines. *Arzneimittelforschung* **2006**, *56*, 405–413.
12. El-Sayed, H.A.; Moustafa, A.H.; Fadda, A.A.; Abd El-Rahman, K.E. Pyrazole and Nicotinonitrile Derivatives Synthesized from Sulfa Drugs, and Their Antibacterial Activity. *Russ. J. Gen. Chem.* **2019**, *89*, 339–347. [CrossRef]
13. Rikagu Oxford Diffraction. *CrysAlisPro*; Agilent Technologies Inc.: Oxfordshire, UK, 2018.
14. Sheldrick, G.M. SHELXT-Integrated Space-Group and Crystal-Structure Determination. *Acta Crystallogr. Sect. A Found. Adv.* **2015**, *71*, 3–8. [CrossRef] [PubMed]
15. Sheldrick, G.M. Crystal Structure Refinement with SHELXL. *Acta Crystallogr. Sect. C Struct. Chem.* **2015**, *71*, 3–8. [CrossRef] [PubMed]
16. Hübschle, C.B.; Sheldrick, G.M.; Dittrich, B. *ShelXle*: A Qt graphical user interface for SHELXL. *J. Appl. Crystallogr.* **2011**, *44*, 1281–1284. [CrossRef] [PubMed]
17. Turner, M.J.; McKinnon, J.J.; Wolff, S.K.; Grimwood, D.J.; Spackman, P.R.; Jayatilaka, D.; Spackman, M.A. *Crystal Explorer 17*; University of Western Australia: Crawley, WA, Australia, 2017. Available online: <http://hirshfeldsurface.net> (accessed on 20 May 2017).
18. Frisch, M.J.; Trucks, G.W.; Schlegel, H.B.; Scuseria, G.E.; Robb, M.A.; Cheeseman, J.R.; Scalmani, G.; Barone, V.; Mennucci, B.; Petersson, G.A.; et al. *GAUSSIAN 09*; Revision A02; Gaussian Inc.: Wallingford, CT, USA, 2009.
19. *GaussView*; Version 4.1; Dennington, R., II; Keith, T.; Millam, J. (Eds.) Semichem Inc.: Shawnee Mission, KS, USA, 2007.
20. Reed, A.E.; Curtiss, L.A.; Weinhold, F. Intermolecular interactions from a natural bond orbital, donor-acceptor viewpoint. *Chem. Rev.* **1988**, *88*, 899–926. [CrossRef]
21. Foresman, J.B.; Frisch, A.E. *Exploring Chemistry with Electronic Structure Methods*, 2nd ed.; Gaussian: Pittsburgh, PA, USA, 1996.
22. Chang, R. *Chemistry*, 7th ed.; McGraw-Hill: New York, NY, USA, 2001.
23. Kosar, B.; Albayrak, C. Spectroscopic investigations and quantum chemical computational study of (E)-4-methoxy-2-[(p-tolylimino) methyl] phenol. *Spectrochim. Acta* **2011**, *78*, 160–167. [CrossRef]
24. Koopmans, T.A. Ordering of wave functions and eigenenergies to the individual electrons of an atom. *Physica* **1933**, *1*, 104–113.
25. Parr, R.G.; Yang, W. *Density-Functional Theory of Atoms and Molecules*; Oxford University Press: New York, NY, USA, 1989.
26. Parr, R.G.; Szentpaly, L.V.; Liu, S. Electrophilicity index. *J. Am. Chem. Soc.* **1999**, *121*, 1922–1924. [CrossRef]
27. Singh, R.N.; Kumar, A.; Tiwari, R.K.; Rawat, P.; Gupta, V.P. A combined experimental and quantum chemical (DFT and AIM) study on molecular structure, spectroscopic properties, NBO and multiple interaction analysis in a novel ethyl 4-[2-(carbamoyl) hydrazinylidene]-3, 5-dimethyl-1H-pyrrole-2-carboxylate and its dimer. *J. Mol. Struct.* **2013**, *1035*, 427–440. [CrossRef]
28. Joe, I.H.; Kostova, I.; Ravikumar, C.; Amalanathan, M.; Cîntă Pînzaru, S. Theoretical and vibrational spectral investigation of sodium salt of acenocoumarol. *J. Raman Spectrosc.* **2009**, *40*, 1033–1038. [CrossRef]

29. Sebastian, S.; Sundaraganesan, N. The spectroscopic (FT-IR, FT-IR gas phase, FT-Raman and UV) and NBO analysis of 4-Hydroxypiperidine by density functional method. *Spectrochim. Acta Part A Mol. Biomol. Spectrosc.* **2010**, *75*, 941–952. [[CrossRef](#)] [[PubMed](#)]
30. Amer, A.; Ayoup, M.S.; Khattab, S.N.; Yassen, S.H.; Langer, V.; Senior, S.; El Massry, A. A regio- and stereo-controlled approach to triazoloquinoxaliny C-nucleosides. *Carbohydr. Res.* **2010**, *345*, 2474–2484.